THE JOURNAL OF PHYSICAL CHEMISTRY C

Article

pubs.acs.org/JPCC

Reversible Hydrophobic/Hydrophilic Adhesive of PS-b-PNIPAAm Copolymer Brush Nanopillar Arrays for Mimicking the Climbing Aptitude of Geckos

Jem-Kun Chen,*[,†] Jing-Hong Wang,[†] Shih-Kang Fan,[‡] and Jia-Yaw Chang[§]

[†]Department of Materials Science and Engineering and [§]Department of Chemical Engineering, National Taiwan University of Science and Technology, 43, Sec 4, Keelung Road, Taipei, 106, Taiwan, Republic of China

[‡]Department of Materials Science and Engineering, National Chiao Tung University, 1001 University Road, Hsinchu, Taiwan 300, Republic of China

ABSTRACT: Inspired by the adjustable adhesive ability of the gecko foot pad, alternately attaching to and detaching from where they climb, we used a fabrication process to generate well-defined pillar patterns of polymerized styrene and successively grafted *n*-isopropylacrylamide (NIPAAm) as thermally responsive terminating of the pillars. By varying the geometry of the patterns including aspect ratio and duty ratio (solid fraction), the respective roles of the geometry the pattern features on the static water contact angle (WCA), hysteresis, adhesive, and friction force at 25 and 50 °C have been systemically investigated. The fabrication strategy exploits surface textures of polystyrene (PS) and thermally responsive terminating of PNIPAAm as the artificial foot pad surface, which could generate alternately ca. 93.9 and 8.7 nN of adhesive force at 25 and 50 °C, respectively. The results indicate that the adjustable adhesive ability of the copolymer brushes could approach the climbing aptitude of a gecko much more closely. We develop a bioinspired artificial analog by using two common methods including atom-transfer radical polymerization (ATRP) and photolithography to adjust adhesion reversibly on a silicon surface. The advantage of the processing strategy described here is the potential to fabricate a device of an artificial foot pad to mimic the climbing aptitude of geckos vividly.

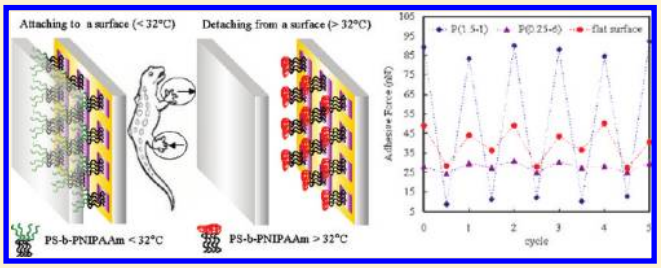

INTRODUCTION

The amazing aptitude of some insects and lizards, such as geckos, to stick readily and rapidly to almost any surface (whether it is hydrophilic or hydrophobic, rough or smooth, or dry or wet) has attracted extensive research interest with respect to the development and application of biomimetic structures. Recent studies have attributed the adhesive ability of geckos to the material properties of their foot pads—sophisticated structural morphology and elasticity coupled with such intermolecular forces as universal van der Waals forces. In the case of small insects and flies, capillary forces have been shown to be responsible for their adhesion. The bioadhesion of these systems has received a lot of experimental and theoretical attention recently,[1,2] especially the adhesion of geckos,[3,4] which are the largest animals able to run on walls and ceilings.[5] Although the adhesion mechanisms of the these animals at the micro- and nanoscales are not completely understood, it has been shown that the ever-present van der Waals forces can be enhanced by capillary forces, either due to capillary condensation from vapor or to natural secretions as occurs with flies. The attachment pads of many insects and geckos are covered with long micro- to nanosized hairs with characteristic geometries and mechanical properties. This remarkable surface topography enables these animals to firmly attach to and easily detach from almost any kind of surface. Much recent work has been directed to a theoretical understanding and modeling of the complex interplay of physical, chemical, and engineering factors behind this adhesion mechanism.[6] However, the role of many of these parameters still remains unclear. Inspired by the above biological systems, various kinds of patterned surfaces with large numbers of regular micro- to nanoscale structures, including cylindrical or conical pillars (columns or posts) with flat, spherical, toroidal, or concave ends, have been designed and fabricated aimed at enhancing adhesion properties.[7,8] Simplified analogs consisting of microsized vertical pillars with modest aspect ratios were obtained by hot-embossing polymer melts with microfabricated masters, or by lithographically structuring resist films.[9,10] Nanosized pillars with higher aspect ratios have also been fabricated by filling nanoporous membranes with polymer solutions or as vertically oriented multiwalled carbon nanotubes.[11,12]

To advance the subject and to provide a rational basis for the creation of superior surfaces, systematic studies of the different parameters are required. So far, mainly the effects of fibril size, for a constant flat punchlike tip shape, have been investigated in

Received: November 29, 2011
Revised: March 1, 2012
Published: March 1, 2012

detail.[4,13] In that study, the principle of contact splitting, which favors a large number of smaller contacts over a small number of large ones,[14] was validated. However, nature provides a variety of contact shapes, ranging from spherical to conical, filamentlike, flat, toroidal, and concave terminals.[15] Recent experimental reports[9] have stressed the significance of shape also in artificial systems; however, in systematic terms, this degree of freedom so far has been largely neglected in the design of artificial analogues. For this purpose, different lithographic and soft-molding methods were combined to fabricate elastomeric surfaces patterned with micropillars of different shapes (flat, spherical, concave, mushroom-type, and spatular terminals) and dimensions. Their adhesion behavior was systematically characterized in terms of tip geometry and pillar radius and compared with theoretical predictions.[16,17] Indeed, a strong effect of contact shape was identified which can overshadow the influence of contact size. Most of these literatures reported approaches to merely pursue extremely high bioattachment or superhydrophobicity and superhydrophilicity of a nanostructured surface.[18,19] Without adjustable adhesive ability, these nanostructed surfaces may stick to a surface firmly, but they could not detach from a surface easily. To mimic a gecko foot pad vividly, the adjustable adhesive ability of simultaneously attaching to and detaching from a surface through internal stimuli is necessary, but not merely high adhesion or an excellent lotus effect.

The use of polymers as building blocks for surface modification allows the preparation of "smart" or responsive surfaces based on conformational changes in the polymer backbones.[20,21] Stable polymer brushes can provide excellent mechanical and chemical protection to the substrate, alter the electrochemical characteristics of the interface, and provide new pathways for the functionalization of silicon surfaces.[22,23] Stimuli-responsive hydrogels, which undergo large reversible volume change in response to changes of environmental factors, are excellent candidates for various chemical or biological detection applications.[24,25] However, to our knowledge, an approach using hydrogel to manufacture more complex structures, closer in design and performance to those in nature, in biomimetic foot pads of lizards, alternately attach to and detach from where they climb, is still lacking in the literature. In a typical diblock copolymer brush structure, one of the blocks is tethered to the surface and the other block stretches away from the surface to interact with the contacting medium.[26] Such chemically grafted polymer layers are inherently more stable than layers formed by physical adsorption or spin coating. The behavior and properties of tethered diblock copolymer brushes are interesting in that because of the different properties of the two blocks (hydrophobicity, flexibility, etc.) the brushes may undergo a structural rearrangement and property change in response to external stimuli.[27,28] In previous study, we reported a fabrication process, involving very large scale integration (VLSI) and oxygen plasma treatment (OPT), to generate well-defined patterns of polymer brushes.[29,30] In this context, we first design a artificial foot pad involving well-defined pillar patterns of polymerized styrene and successively grafted *n*-isopropylacrylamide (NIPAAm) as the thermally responsive terminal of the pillars to generate high and low adhesive force through temperature tuning for mimicking the climbing aptitude of geckos. Not merely pursuing high adhesion or excellent lotus effect, adjustable adhesive ability is focused on in this work, including the fabrication of a series of copolymer brush pillars with systematically controlled geometry on silicon wafers and testing of the contact surfaces possessing stimuli-responsive hydrogels. The pillar arrays of block copolymer brushes were made by polystyrene (PS) and PNIPAAm prepared via surface-initiated consecutive atom-transfer radical polymerization (ATRP) on initiator-immobilized silicon surfaces.[31,32] PNIPAAm is the best known of the thermoresponsive polymers, displaying reversible solubility changes in response to temperature in the vicinity of 32 °C.[24] The width (w), the height (h), spacing (i), duty ratio ($d = i/w$), and the aspect ratio ($a = h/w$) of the pillars were systematically and independently varied as shown in Figure 1. The influence of these parameters on the static water contact angles (WCAs), hysteresis, adhesive force, and friction properties of the surfaces are described and compared with theoretical predictions. The discussion of the results presented in this paper will contribute to a novel understanding and creativity of the relevant factors responsible for adjustable adhesive ability in biological systems and will guide the device design of bioinspired artificial analogues.

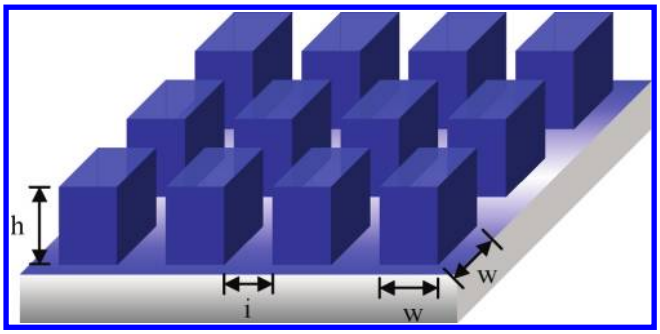

Figure 1. Design parameters for the pillar array of PS-b-PNIPAAm copolymer brushes.

EXPERIMENTAL SECTION

Materials. Single-crystal silicon wafers, Si(100), polished on one side (diameter: 6 in.) were supplied by Hitachi, Inc. (Japan) and cut into 0.6 in. × 0.6 in. samples. The Si substrates were immersed in hydrofluoric acid solution (10 wt %) for 10 min at room temperature to remove the silicon oxide film. The hydrofluoric acid-treated substrates were successive immersed in the mixture of H_2SO_4 and H_2O_2 (2:1 mol %) for 5 min and subsequently rinsed with doubly distilled water a minimum of five times to oxidize the Si. *N*-Isopropyl acrylamide (NIPAAm, Acros Organics Co) was recrystallized from a toluene/hexane solution (50% v/v) and dried under vacuum prior to use. Styrene (Acros Organics Co) was washed three times with a 5 wt % sodium hydroxide solution and twice with distilled water. After drying with anhydrous magnesium sulfate, the monomer was purified by distillation under reduced pressure and stored in a refrigerator immediately after distillation. Other materials used for graft polymerization, 3-aminopropyltriethoxysilane (AS) and 2-bromo-2-methylpropionyl bromide (BB), copper(I) bromide, copper(II) bromide, triethylamine (TA), and 1,1,4,7,7-pentamethyldiethylenetriamin (PMDETA), were purchased from Acros Organics Co. PMDETA, AS, and BB were purified through vacuum distillation prior to use. All other chemicals and solvents were of reagent grade and purchased from Aldrich Chemical Co.

dx.doi.org/10.1021/jp301068k | J. Phys. Chem. C 2012, 116, 6980−6992

Preparation of the Copolymer Pillar Array of PS-b-PNIPAAm-Grafted Silicon. The basic strategy for the fabrication of the patterned PS-b-PNIPAAm copolymer brushes using the VLSI process is from the previous study as shown in Figure 2.[33] (A) The Si wafer was treated with hexamethyldisilazane (HMDS) in a thermal evaporator (Track MK-8) at 90 °C for 30 s to transform the hydroxyl groups on the surface of wafer into an inert film of $Si(CH_3)_3$ groups. The photoresist was spun on the HMDS-treated Si wafer at a thickness of ca. 780 nm. Contact hole arrays possessing various periods and resolutions on the photoresist were successively patterned by lithography process. (B) The sample was then subjected to OPT to form hydroxyl groups from the HMDS-treated surface. OPT caused the bottom surface to become chemically modified (strongly hydrophilic or polar) only in the areas not covered by the photoresist.[34] (C) To immobilize the ATRP initiator, the Si substrate was immersed in a 0.5% (w/v) solution of AS in toluene for 2 h at 50 °C. The AS units assembled selectively onto the bare regions of the bottom Si surface after OPT, where it reacted with Si−O and Si−O−O species. The sample was immersed in both of 2% (v/v) solution of BB and TA in toluene for 8 h at 20 °C. After reaction, the wafers were placed in a Soxhlet apparatus to remove any nongrafted material. This procedure resulted in a surface patterned with regions of AS−BB for ATRP and regions of photoresist. ATRP of monomer mixture including 80 mol % styrene and 20 mol % 1,4-divinylbenzene (DVB) was carried out according to a previously reported method.[23,35] DVB, which contains two reactive vinyl groups, is an excellent cross-linker for the preparation of 3-D polymer networks. For the preparation of cross-linked PS brushes on the Si−AS−BB surface, the mixture monomer, Cu(I)Br, $CuBr_2$, and PMDETA were added to toluene. The solution was stirred and degassed with argon for 15 min at 90 °C. The solution was successively transferred to a flask containing Si−AS−BB silicon wafers, and extra BB was added by syringe. Polymerization of the monomer mixture was allowed to proceed at 70 °C for 48 h inside the square hole array of photoresist to generate pillars as the basic structure of biomimetic surfaces. Afterward, the wafers were taken out of the polymerization solution and rinsed thoroughly with toluene. To remove physically adsorbed polymer, the wafers were Soxhlet extracted with dichloromethane for 24 h, cleaned ultrasonically in dichloromethane, and finally dried under a flow of nitrogen. (D) The Si-PS surfaces were used as macroinitiators for the subsequent surface-initiated ATRP of PNIPAAm to produce diblock copolymer brushes. Surface-initiated ATRP grafting of NIPAAm was carried out in a glass vessel purged with nitrogen. NIPAAm, PMDETA, and Cu(I)Br, $CuBr_2$, were dissolved in dimethylformamide (DMF). The reaction solution was sonicated for 2 min and then was added to the glass vessel in which the macroinitiator-functionalized wafers were placed. Polymerization was carried out at room temperature under nitrogen purging for 12 h inside the square hole array of photoresist for attachment of the thermally responsive property on the contact regime of pillars. After the desired period of time, the obtained PS-b-PNIPAAm-grafted silicon wafers were removed from the solution, rinsed with abundant deionized water to remove unreacted monomer and PNIPAAm that was not grafted, and then dried under a flow of nitrogen. (E) Finally, the remaining photoresist was removed from the PS-b-PNIPAAm-grafted silicon surface by rinsing with slight basic aqueous solution, leaving behind the chemically nanopatterned PNIPAAm-b-PS brush surface. The surfaces were then dried under vacuum at room temperature for 20 min. Surfaces were treated with different solvents to investigate possible surface rearrangement. Water was chosen as a good solvent for the PNIPAAm segment, and cyclohexane was chosen as a good solvent for the PS segment. The PS-b-PNIPAAm surfaces were immersed in 20 mL of deionized water at room temperature or cyclohexane at 40 °C for 1 h.

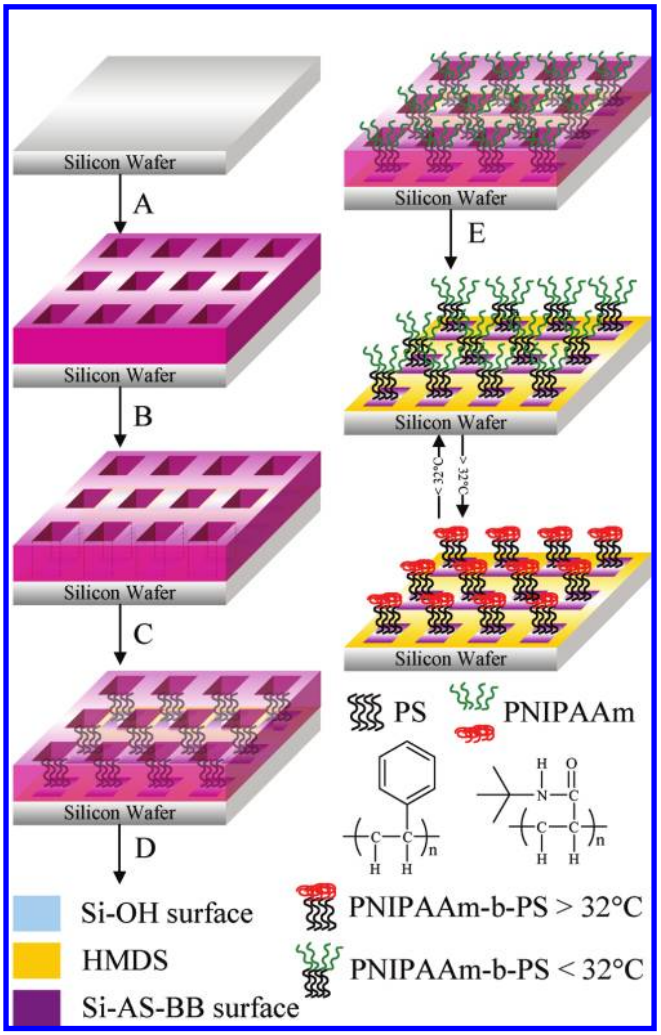

Figure 2. Schematic representation of the process used to fabricate chemically nanopatterned surfaces of PS-b-PNIPAAm brushes. (A) Si wafer treated with HMDS in a thermal evaporator, photoresist spin-coated onto the Si surface presenting $Si(CH_3)_3$ groups, and lithography process used to pattern the photoresist as hole arrays with various aspect and duty ratios on the surface. (B) OPT used to chemically modify the exposed regions presenting $Si(OCH_3)_3$ groups and to convert the topographic photoresist pattern into a chemical surface pattern. (C) AS selectively assembled onto bare regions of the Si surface and BB successively reacted with assembled AS onto bare regions of the Si surface to form the initiator. (D) Sample grafting via surface-initiated ATRP of a mixture of styrene and DVB from the functionalized areas of the patterned SAM as pillar arrays of PS brushes. (E) Sequentially, the object grafting via surface-initiated ATRP of NIPAAm from the macroinitiator on the contact area of the pillars to generate PS-b-PNIPAAm copolymer pillars. (F) Finally, photoresist removed through treatment with slight base aqueous solution. The pillar arrays of the copolymer brushes on the surface exhibited thermally dependent behavior on adhesion between 25 and 50 °C.

dx.doi.org/10.1021/jp301068k | J. Phys. Chem. C 2012, 116, 6980−6992

The samples were removed from the solvent and dried in a flow of nitrogen, followed by water contact angle measurement. The chemical composition of the modified silicon surfaces was determined with a photoelectron spectrometer (XPS) (XPS; Scientific Theta Probe, UK). The thickness of the copolymer grafts on the silicon substrate was measured with ellipsometry (SOPRA SE-5, France) and high resolution scanning electron microscope (HR-SEM, JEOL JSM-6500F, Japan).

Surface Characterization. To investigate the surface morphologies of various patterns of PS-b-PNIPAAm brush, the samples were immersed in deionized water for 3 h and then lyophilized prior to Atomic force microscopy (AFM) examination. AFM is a suitable technique for surface morphology, friction and wear characterization at the nanoscale as it has the ability to measure material properties with high spatial resolution.[36] Nanofriction and adhesive force was measured experimentally by an AFM/FFM (Veeco Dimension 5000 Scanning Probe Microscope), using the contact mode. Commercially available rotated monolithic silicon probe, symmetric tip shape with a nominal spring constant of 3 N/m, and a coated tip with a curvature radius of less than 10 nm was employed. Friction forces were obtained from friction-load line on each surface with a scan frequency of 1 Hz and a scan size of 80 × 80 μm^2. The output voltages were directly used as frictional forces. No attempt was made to calibrate the torsion force constant. Repeated measurements were within 1% of the average value for each sample. Adhesive force which is also called pull-off force was obtained from the force−distance curve and was calculated by F = KcZp.[37] Where, Kc is the force constant of cantilever, and Zp is the vertical displacement of the piezotube. For all measurements, the same tip was used in this study. All the measurements were performed at room temperature with a relatively humidity of 25−35%. Repeated measurements were within 5% of the average value for each sample. The surface roughness (rms) was calculated from the roughness profiles.

The static WCAs of the functionalized silicon surfaces were measured using the sessile drop method on an optical WCA meter. The WCA was determined by fitting a Young−Laplace curve around the drop. The experiment was performed under normal laboratory ambient conditions, 25 °C, and 30% relative humidity. The mean value was calculated from at least 10 individual measurements and the measurement error was less than 3°. In addition, it is well-known that a heterogeneous surface (chemically or geometrically) usually shows contact angle hysteresis.[38] That is, for a geometrically rough surface, contact angle hysteresis originates primarily from the rough contact interface that depends upon the contact area of water with the structured surface. The earliest works to model liquid drops on a roughness surface can be contributed to Wenzel[39] and Cassie.[40] In this case, liquid fills up the rough surface to form a completely wetted contact with the surface, as illustrated in Figure 3a, and this phenomenon is known as the Wenzel state. On the other hand, a liquid droplet sits on a composite surface composed of solid and air, as illustrated in Figure 3b, which is also known as the Cassie state. It is well-understood that there is no unique contact angle to characterize any given surface. The observed equilibrium contact angles always fall between the advancing and receding contact angles. The contact angle hysteresis $\Delta\theta$, defined as the difference between advancing and receding contact angles ($\Delta\theta = \theta_{adv} - \theta_{rec}$), can be used to conclude the state of a liquid droplet. If the contact angle hysteresis is small, then the droplet would be at the Cassie state. On the other hand, if the contact angle hysteresis is large, then the droplet would be at the Wenzel state. This implies that the contact angle hysteresis is responsible for the pinning of liquid droplets on a surface.

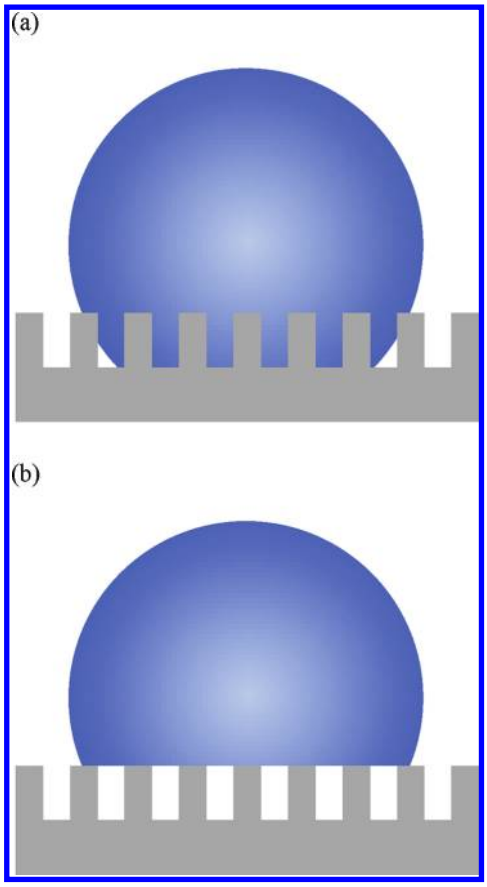

Figure 3. Schematic illustrations of a liquid droplet at Wenzel state (a) and at Cassie state (b).

RESULTS AND DISCUSSION

Formation of PS-b-PNIPAAm Brushes on Silicon Substrates via Surface-Initiated ATRP. The general process for the formation of PS-b-PNIPAAm block copolymer brushes on a silicon surface by ATRP is illustrated in Figure 2. First, a homogeneous, dense monolayer of initiator was immobilized on the silicon surface. Si-ATRP of a mixture of styrene and DVB was successively carried out by immersing the initiator modified silicon. The resulting PS-grafted layer had a thickness of ∼226 nm as determined by ellipsometry, more than the value reported elsewhere.[41] The results ascribe that the Si-ATRP of styrene was carried out inside the square hole array of potoresist. In general, the grafting species on surface-tethered polymer brush chain with lower degree of freedom deactivated due to the entanglement of polymer chains.[31] The halogen groups of chain end consecutively stocked on the upper part of the polymer brushes due to the besieging of the photoresist, enhancing the reactivity of halogen groups. The ATRP of NIPAAm was then carried out in DMF with the grafted PS brushes as the macroinitiator. Free BB initiator was added to the polymerization medium to generate a sufficient concentration of the deactivator copper(II) species; this is necessary for the formation of homogeneous films with grafts of controlled length, especially in the beginning stages of the ATRP process. In this work, an increase in thickness of ∼76 nm

dx.doi.org/10.1021/jp301068k | J. Phys. Chem. C 2012, 116, 6980−6992

compared to the initial PS layer indicated the formation of PNIPAAm blocks. These results imply the activity of the grafting species (halogen group) in ATRP is not deactivated during the polymerization process. Changes in the chemical composition of silicon surfaces after grafting were determined from XPS data. Figure 4a and b shows survey spectra of the PS- and PS-b-PNIPAAm-grafted surfaces, respectively. For the PS-grafted surface, only the C element was observed, suggesting that the surface was completely covered with a PS layer. Because the thickness of the grafted PS layer,~226 nm, was much more than the sampling depth of the XPS measurement (~10 nm), the N 1s and O 1s components of initiator could not be discerned after the addition of the PS block. The high-resolution C 1s spectra are also shown in Figure 4a (inset). These were curve fitted using a peak with binding energies of 284.15 eV, attributable to chemical bonding environments C—C/H. Because PNIPAAm is composed mainly of C, H, O, and N elements, it is expected that the N 1s and O 1s components should appear after the addition of the PNIPAAm block; indeed, the N 1s and O 1s peak appeared apparently in Figure 4b. The high-resolution C 1s spectra are also shown in Figure 4b (inset). These were curve fitted using peaks with binding energies of 284.2, 285.8, and 287.6 eV, attributable to chemical bonding environments C—C/H, C—N, and C═O, respectively. Static WCA measurements indicated the wettability of the functionalized silicon surfaces at various stages in previous study.[42,43] The PS modified silicon substrate was strongly hydrophobic (contact angle ~88°). This compares to the closed value for silicon modified with PS alone.[44] It possessed thermoresponsiveness after modification by PNIPAAm, with angles of 41.8° at 25 °C and 82.1° at 50 °C. This strong temperature dependence of surface wettability further demonstrated the formation of a PNIPAAm layer of the copolymer.

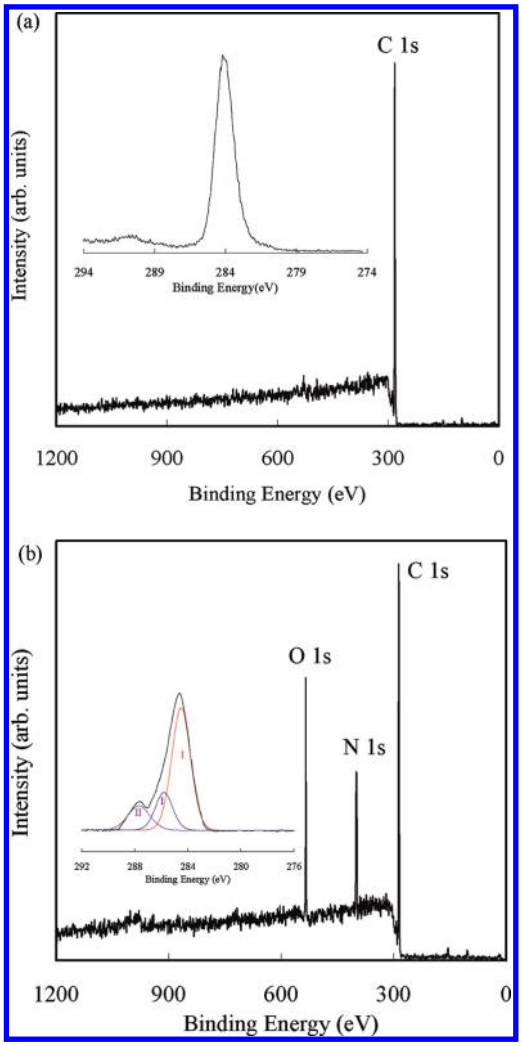

Figure 4. XPS survey spectra and high-resolution C 1s spectra (inset) of (a) PS- and (b) PS-b-PNIPAAm-grafted surfaces. The peak assignments are (I) C—C/H, (II) C—N, and (III) C═O.

Surface Morphology and Characterization. The regular pillar structure used in this study is schematically illustrated in Figure 1. For convenience, the notation P(a–d) is applied to describe the microstructure with aspect ratio ($a = h/w$) and duty ratio ($d = i/w$) for $w \times w$ nm square pillars separated by a distance i nm and the pillar height h nm. All the detailed dimensions of these pillars were determined by AFM. The duty ratio and the aspect ratio of the pillars were systematically and independently determined. Roughness in terms of rms was determined by the analysis software of the AFM, and the pillar-to-pillar distance found by analysis of cross-section lines was taken in different directions from the images. Pillar fractional surface coverage f (%) was determined by the following equation:

$$f(\%) = \frac{NS_{\text{pillar}}}{S_{\text{scan}}} = \frac{Nw^2}{S_{\text{scan}}}$$

Where, N is the number of pillars; S_{scan} = the AFM scan area. According to the above calculation, the pillar fractional surface coverage f (%) relates to the duty ratio. All geometrical parameters including the h, w, f, a, d, and surface roughness are summarized in Table 1.

Table 1. Geometrical Parameters of PS-b-PNIPAAm Copolymer Brush Patterned Surfaces with Micro-/Nanopillars Used in Our Experiment

		surface roughness rms[a] (nm)						pillar fractional surface coverage[a] f (%)					
width (nm)	aspect ratio ($a = h/w$)	$d = 1$	$d = 2$	$d = 3$	$d = 4$	$d = 5$	$d = 6$	$d = 1$	$d = 2$	$d = 3$	$d = 4$	$d = 5$	$d = 6$
200	1.52	83.2	66.6	90.9	70.9	63.8	46.8	47.3	31.9	13.7	7.6	5.3	2.9
400	1.01	145.5	132	84.2	65.4	70	45.2	45.8	30.5	12.5	7.0	5.0	2.6
600	0.76	150.3	135.9	84.4	67.4	65.8	70.9	44.7	26.7	11.1	6.6	4.9	2.7
800	0.50	146.5	132	105	80.2	66.2	59.7	44.8	25.0	11.5	6.2	4.2	2.7
1000	0.38	145.2	96.4	110.1	70	55.5	65.4	44.4	25.2	11.3	6.3	4.0	2.8
1200	0.25	135.5	111.2	88.2	80.7	66	72	44.6	25.0	11.2	6.1	3.9	2.7

[a]Determined from AFM by scanning area of 10 μm × 10 μm.

dx.doi.org/10.1021/jp301068k | J. Phys. Chem. C 2012, 116, 6980–6992

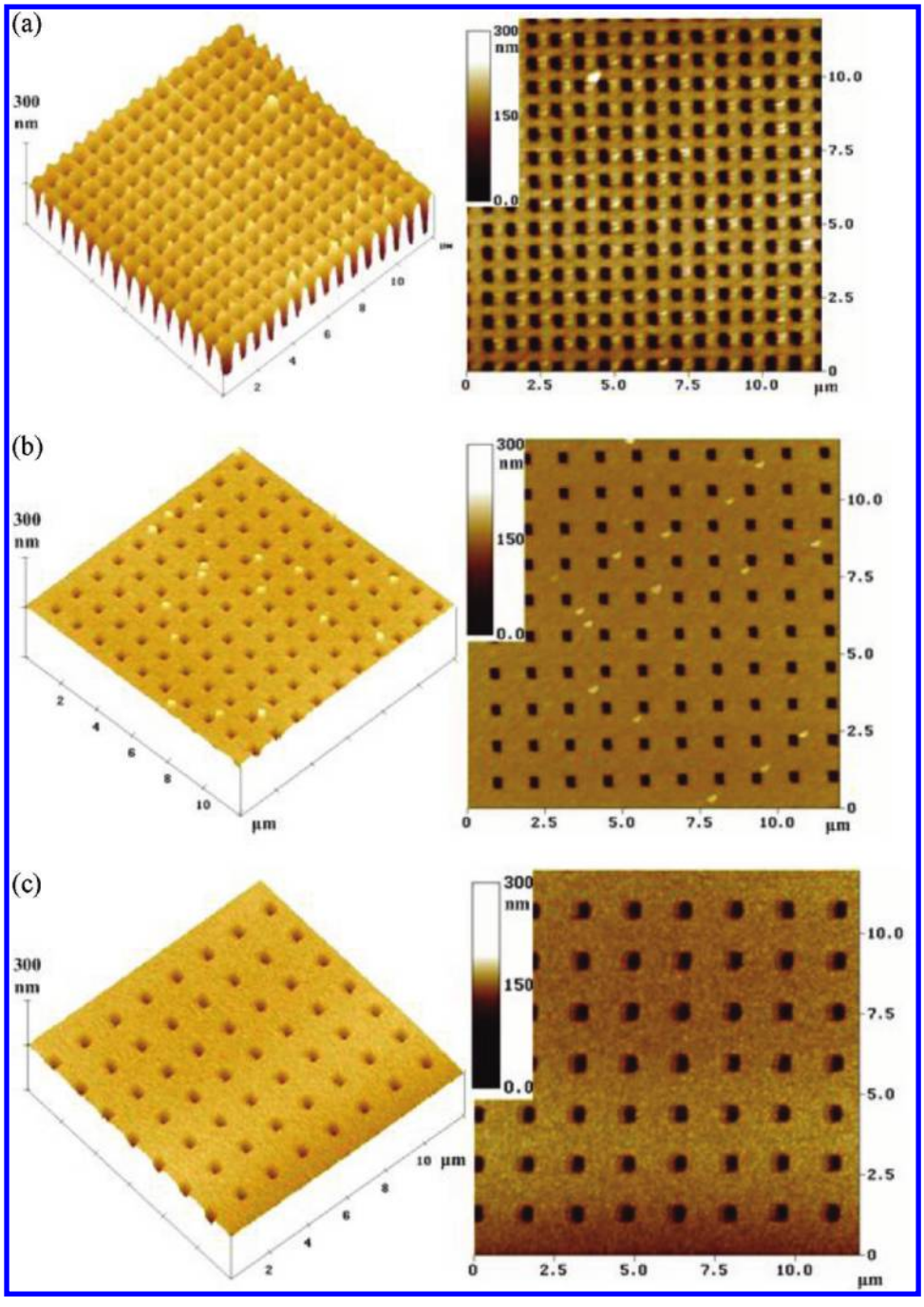

Figure 5. 2D and 3D AFM height images (10 μm × 10 μm) of 400 nm resolution contact hole arrays possessing duty ratio of (a) 1, (b) 2, and (c) 3, generated by the lithography process, respectively.

2D and 3D AFM topographic images of photoresist templates possessing square contact hole arrays with 400 nm resolution are depicted in Figure 5. The intervals between square hole arrays were arranged in order of duty ratios from 1 to 3 as shown in Figure 5a−c, respectively. As seen form Figure 5, hole textures of the photoresist with the same depth but varying fractional surface coverage were clearly shown. We treated these square hole array by OPT to create hydroxyl group on the bottom surface of the array. The PS-b-PNIPAAm copolymer brush was grafted sequentially from the bottom surface of these square hole arrays by ATRP as pillar arrays. We used AFM to visualize the topographies of the PS-b-PNIPAAm brush pillar with various structures. 2D and 3D AFM topographic images of the pillar array of PS brush and PS-b-PNIPAAm brush pillar including duty ratios from 1 to 3 were depicted in Figures 6 and 7, respectively. As depicted in Figure 6, the PS pillar arrays were fabricated successfully that have uniform height (226 nm) and width (400 nm) but different area density. After grafting PNIPAAm on the contact area of the pillar array, the height increase ca. 76 nm, identified as the thickness of the PNIPAAm. The width of the PS-b-PNIPAAm pillar was over 400 nm due to swelling of the copolymer brushes by removing photoresist with slight basic aqueous solution in final stage.

Wetting/dewetting ability is an important property for a solid surface because it plays a crucial role in many biomimetic

dx.doi.org/10.1021/jp301068k | J. Phys. Chem. C 2012, 116, 6980−6992

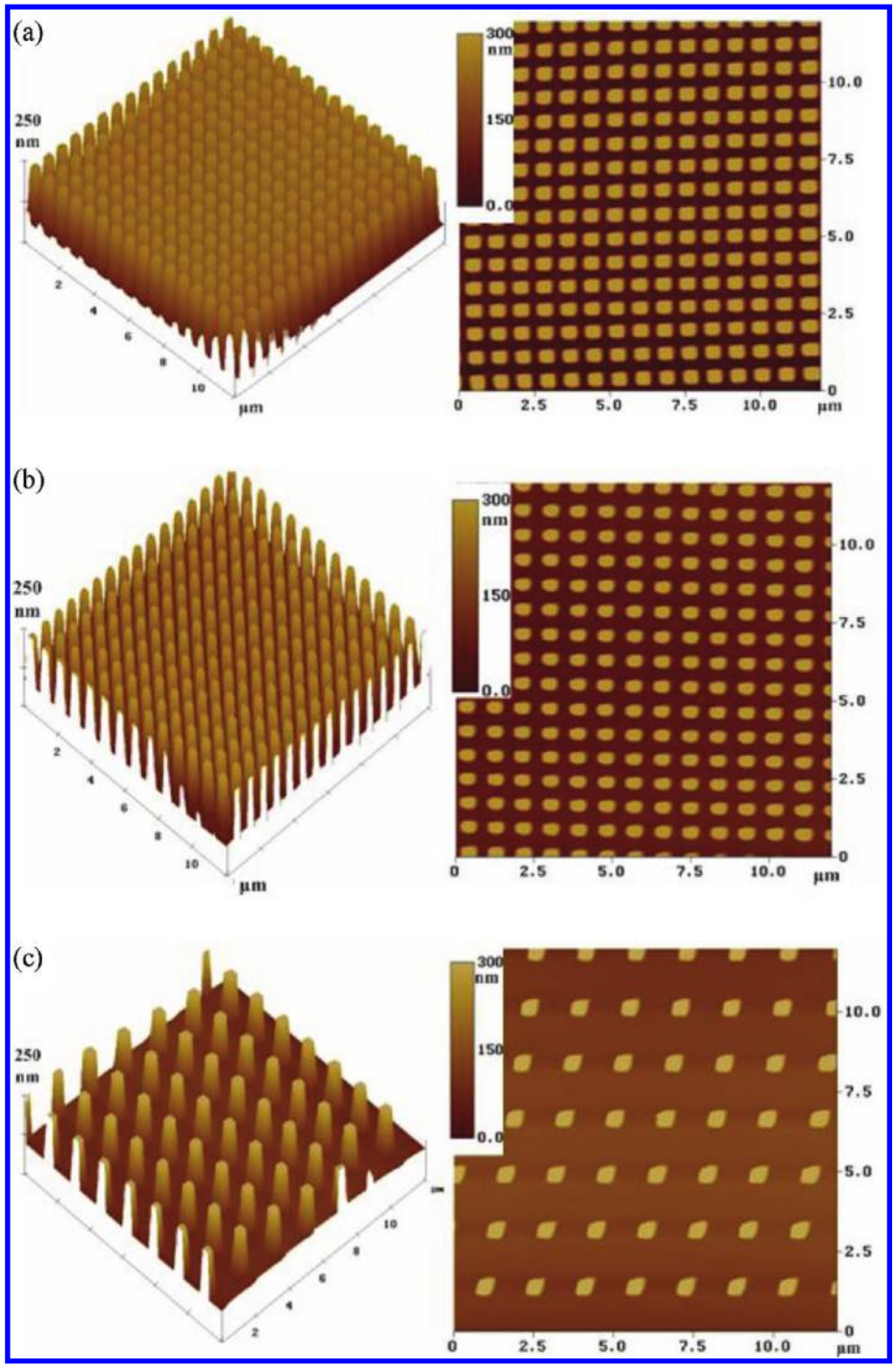

Figure 6. 2D and 3D AFM height images (10 μm × 10 μm) of 400 nm resolution pillar arrays of tethered PS brush possessing duty ratio of (a) 1, (b) 2, and (c) 3, grafted from a modified-Si surface by ATRP, respectively.

applications, which is determined by measuring static WCAs at equilibrium states. It has been reported that the wettability of PNIPAAm-grafted surfaces undergoes a temperature-dependent transition near the LCST (~32 °C) of PNIPAAm.[41] Below the LCST, the PNIPAAm chains are strongly hydrated with an extended conformation, but when heated to above the LCST, the polymer undergoes a phase transition to a collapsed morphology due to dehydration. This response will be modified when NIPAAm is copolymerized with other monomers that are either hydrophilic or hydrophobic.[45] In this work, static WCAs of flat and nanopillar surfaces of PS-b-PNIPAAm brushes below and above the LCST were measured, respectively. It can be seen in Figure 8a that both of the Si-PS on flat and nanopillar surfaces remained similar static WCAs at 25 and 50 °C. Apparently, the pillar structure of PS brush enhanced the hydrophobic property on the surface, consistent with other reports.[46] After block copolymerization with PNIPAAm, the PS-b-PNIPAAm copolymer brush exhibited higher WCAs at 50 than at 25 °C because of the addition of PNIPAAm segments, corresponding other reports.[47] We defined the difference of the static WCAs at 25 and 50 °C as a thermally responsive efficiency of static WCA ($\Delta\theta_{eff} = WCA_{50°C} - WCA_{25°C}$) during

dx.doi.org/10.1021/jp301068k | J. Phys. Chem. C 2012, 116, 6980−6992

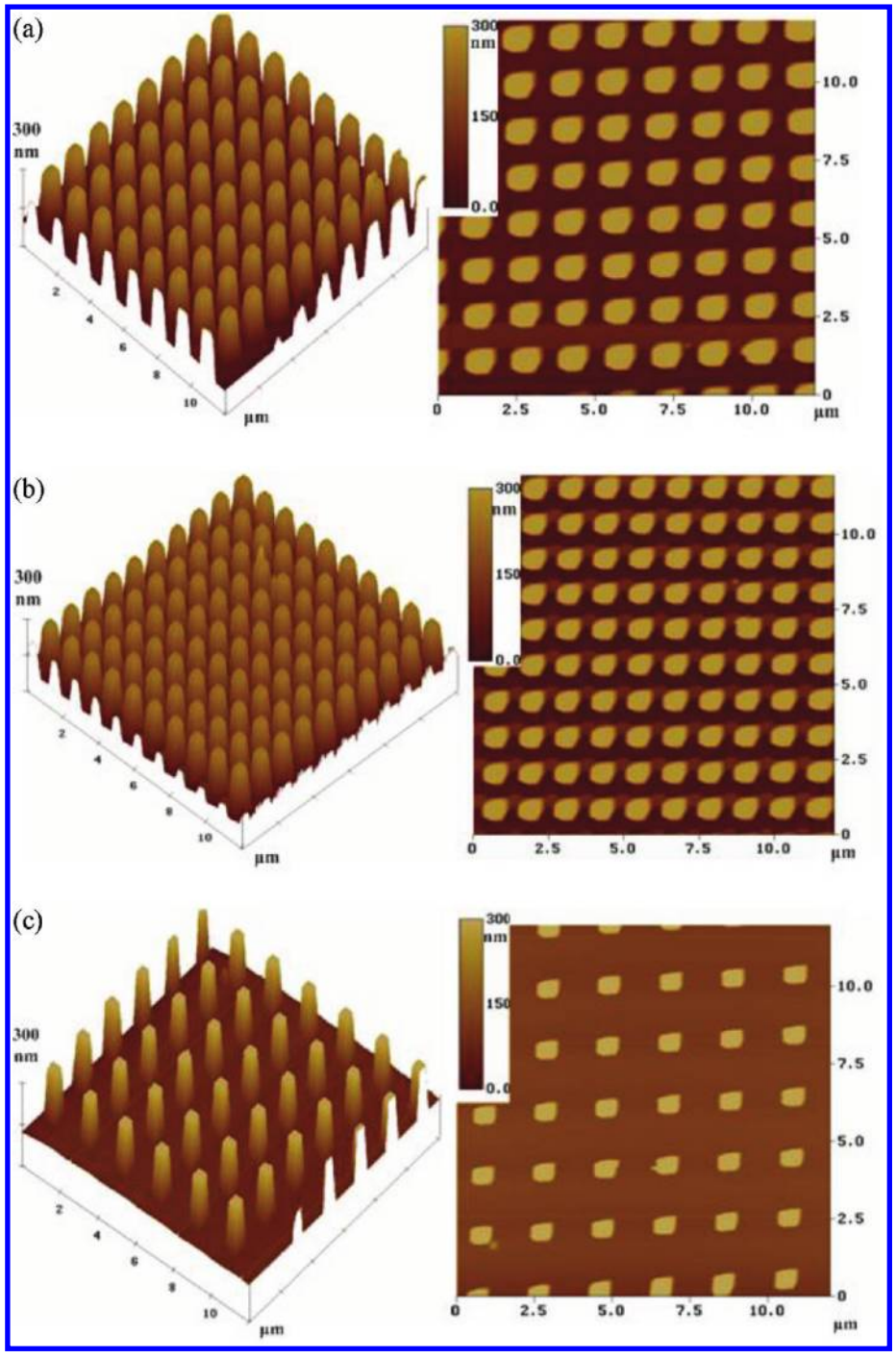

Figure 7. 2D and 3D AFM height images (10 μm × 10 μm) of 400 nm resolution pillar arrays of tethered PS-b-PNIPAAm brush possessing duty ratio of (a) 1, (b) 2, and (c) 3, grafted from the PS macroinitiator as contact area by ATRP, respectively.

the phase transition. The P(1.5−1) of the PS-b-PNIPAAm possessed the lower static WCA than that of flat surface at 25 °C due to the capillary/meniscus forces.[48] Figure 8b and c shows the variation of static WCAs for the pillar structures with duty ratios from 1 to 6 as a function of aspect ratios at 25 and 50 °C, respectively. At 25 °C, the static WCAs of the PS-b-PNIPAAm-modified pillar decreased obviously with increase of the aspect ratio, especially the duty ratios from 1 to 3.(Figure 8b) At 50 °C, the copolymer nanopillar undergoes a phase transition to a collapsed morphology due to dehydration. The static WCAs on the copolymer nanopillar surface increased obviously with the aspect ratio, especially the duty ratios from 1 to 3.(Figure 8c) However, the static WCAs of the PS-b-PNIPAAm pillar show the lower thermally responsive efficiency of static WCAs when the duty ratios are from 4 to 6 under tuning temperature between 25 and 50 °C. Note that liquid fills up the rough surface to form a completely wetted contact with the surface, causing the independence of static WCAs of tethered PS-b-PNIPAAm on the aspect ratio. The results suggest that the wettability of a solid surface depends on both the surface structure and the surface property. The static WCA of P(1.5−1) of tethered PS-b-PNIPAAm brushes increased substantially from 14.9 ± 4° to 118.5 ± 4° upon increasing the temperature from 25 to 50 °C; it returned to 15.6 ± 4° after

dx.doi.org/10.1021/jp301068k | J. Phys. Chem. C 2012, 116, 6980−6992

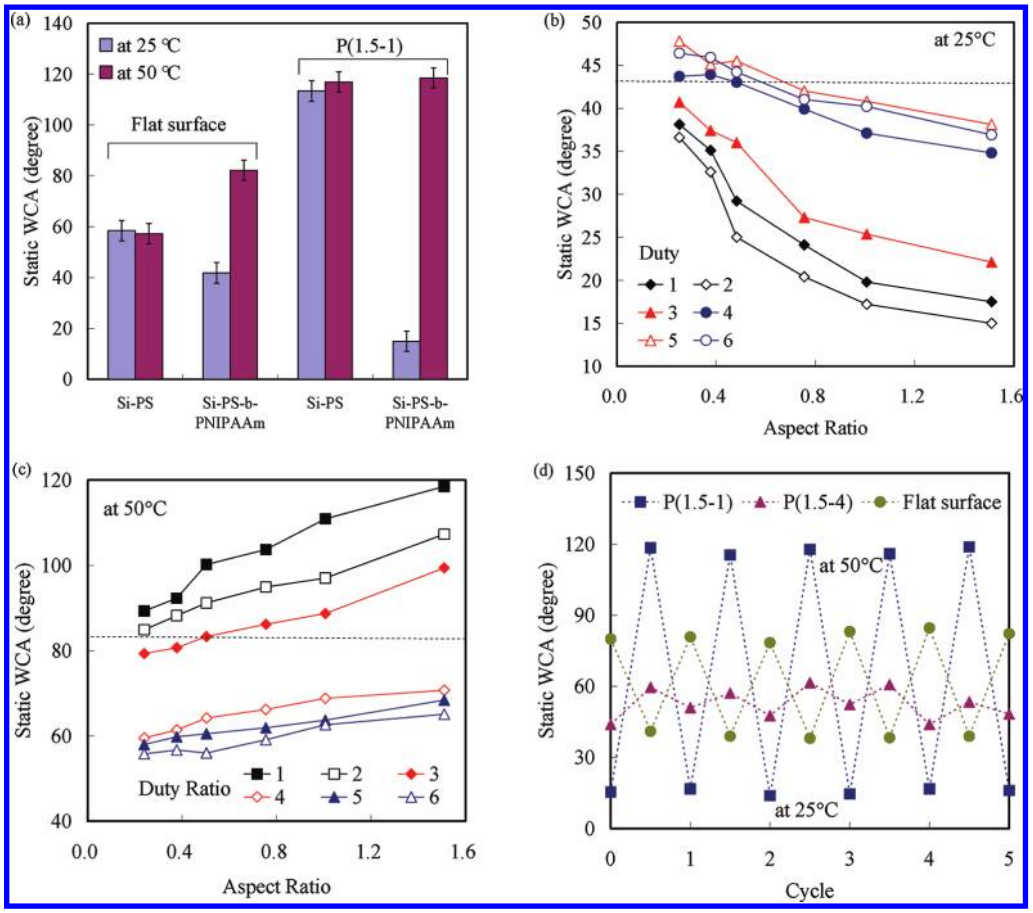

Figure 8. (a) Static WCAs of flat and P(1.5−1) of Si-PS, and Si-PS-b-PNIPAAm surfaces at 25 and 50 °C. Data consist of the mean ± standard error (n = 3). Variation of the static WCAs on the PS-b-PNIPAAm pillar surfaces as a function of the aspect ratios at (b) 25 and (c) 50 °C. The dashed lines in b and c represent the static WCAs on flat PS-b-PNIPAAm surface at 25 and 50 °C, respectively. (d) Static WCAs of P(1.5−1), P(1.5−4), and flat surface of the tethered PS-b-PNIPAAm after 5 cycles tuning temperature between 25 and 50 °C.

decreasing temperature from 50 to 25 °C. For the nanopillar substrate including P(1.5−1) and P(1.5−4), tethered PS-b-PNIPAAm brushes on the surface exhibited thermally dependent behavior from 25 to 50 °C. This behavior was reversible for 5 cycles as shown in Figure 8d. The P(1.5−1) of tethered PS-b-PNIPAAm brushes exhibited the largest thermally responsive efficiency of static WCAs due to the highest density of the pillars. These results suggest that the thermally responsive efficiency of static WCAs could be enhanced by the PS-b-PNIPAAm pillar array.[41]

Furthermore, the dynamic WCAs (advancing and receding contact angles) on these pillar structure are recorded to obtain the hysteresis at 25 and 50 °C, respectively. Note that the hysteresis is independent of the surface roughness at the Cassie state. On the other hand, the hysteresis increases (or decreases) with an increase in the surface roughness at the Wenzel state. There is a discontinuity of the hysteresis when the transition between the Wenzel state and the Cassie state occurs. It is believed that the hysteresis on a surface is strongly associated with roughness of the surface. A liquid droplet sits on a composite surface composed of solid and air. In this case, the system falls into the Wenzel state.(Figure 3a) Increasing of surface roughness (aspect ratio and fractional surface coverage) enhances the surface hydrophobicity. This is because with the increasing surface roughness, air may be trapped in the cavities of a rough surface, resulting in a composite solid−air−liquid interface, as opposed to the homogeneous solid−liquid interface. The system falls into the Cassie state (Figure 3b). Therefore, the solid fraction (roughnes) could be an index for the fraction of the three-phase contact line on the solid surface when the transition between the Wenzel state and the Cassie state occurs. Theoretical surface roughness R_a was calculated by assuming a smooth cutting surface to evaluate the hysteresis and using the following relations:

$$R_a = 1 + \frac{4wh}{(w+i)^2}$$

Figure 9 displays the WCA hysteresis of the PS-b-PNIPAAm brush pillars plotted as a function of R_a on the nanotexture including duty ratio of 1, 3, and 5 at 25 and 50 °C. At both of 25 and 50 °C, the hysteresis remains almost constant for the nanotexture possessing duty ratio of 1, suggesting this system consecutively belongs to the Cassie state under temperature tuning. In these pillars of PS-b-PNIPAAm, there is a dramatic change in the hysteresis from 25 to 50 °C for the pillars with duty ratio of 3. The hysteresis for the nanostructure possessing duty ratio of 3 increases rapidly with an increase in the roughness at 25 °C as shown in Figure 9. However, the hysteresis remains almost constant for the nanotexture with duty ratio of 3 at 50 °C due to the collapse of the PNIPAAm on the contact area, suggesting the system transited from Wenzel state to Cassie state under tuning temperature from 25 and 50 °C. The observation suggests that there is a thermally responsive hysteresis right at the transition point between the

dx.doi.org/10.1021/jp301068k | J. Phys. Chem. C 2012, 116, 6980−6992

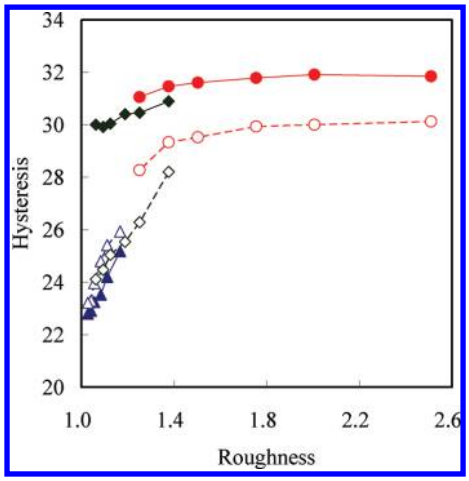

Figure 9. (a) Variation of the WCA hysteresis calculated from advancing/receding contact angle of a water droplet on pattern surfaces at fixed duty ratios (d = 1, 3, 5) as a function of the surface roughness. The open symbols stand at 25 °C and filled symbols stand at 50 °C: d = 1 (circle), d = 3 (triangle), and d = 5 (square).

Wenzel state and Cassie state for the nanotexture with duty ratio of 3. However, note that the hysteresis increases substantially as the roughness increases for the nanotexture with duty ratio of 5 at both of 25 and 50 °C without the transition behavior between the Wenzel and the Cassie state under temperature tuning. The results suggest that the transition behavior between the Wenzel and Cassie states under temperature tuning solely occurs at the structure of P(1.5−3). Without nanopillar structure, the PS-b-PNIPAAm thin film on the flat surface exhibited the lowest hysteresis, and the hysteresis remains almost constant at 25 and 50 °C. With nanopillar structure, the hydrophilic or hydrophobic property of PS-b-PNIPAAm pillars caused the movement of a drop on a surface, strongly associated with the movement of the three-phase (air−liquid−solid) contact line. Attaching thermally responsive property with copolymer grafting, PNIPAAm has terminal groups, which are thermally responsive, would generate switching property on contact mode between pillar and surface (Wenzel and the Cassie state). By controlling these factors and varying them independently, we can design a bioinspired artificial analogue possessing switchable contact interface.

Thermally Switchable Adhesive Force of Tethered PS-b-PNIPAAm Copolymer Pillar. Adhesion is generally measured by the amount of force necessary to separate two surfaces in contact. The geometry of the adhesion tests with a representative experimental force−distance curve obtained on patterned surfaces with pillars of Si-PS-b-PNIPAAm along 80 μm of scanning distance is depicted in Figure 10a. During loading, the curves initially show a nonlinear response related to the change in the stiffness as the number of pillars in contact increased. No significant approach-retraction hysteresis could be noticed, indicating that the deformation of the sample is predominantly elastic, and viscoelastic effects, while present,

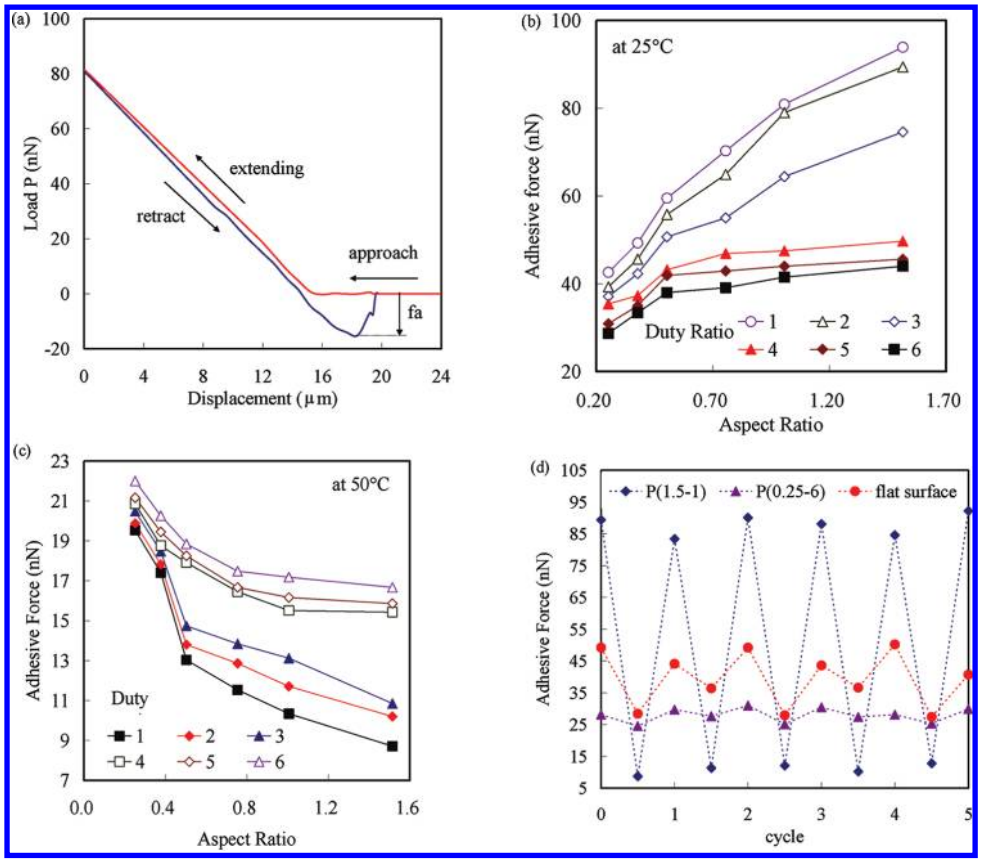

Figure 10. (a) Load−displacement curve obtained from a patterned surface with d = 1 and a = 1.5. A sawtooth profile can be observed during retraction before pull-off occurs. (b and c) Changes in adhesive forces of the tethered PS-b-PNIPAAm pillar with duty ratio from 1 to 6 plotted as a function of aspect ratio at (b) 25 and (c) 50 °C, respectively. (d) Adhesive forces of P(1.5−1), P(0.25−6), and flat surface of the tethered PS-b-PNIPAAm brushes after 5 cycles tuning temperature between 25 and 50 °C.

dx.doi.org/10.1021/jp301068k | J. Phys. Chem. C 2012, 116, 6980−6992

can be neglected. During retraction, the curves showed several points of instability where the force changed abruptly. The resulting sawtooth profile was associated with isolated detachment events of the peripheral pillars in the contact area. These effects were not seen when measuring adhesion to a planar surface. The final detachment event gives the value of the adhesive force (P_{ad}). The influence of the fabrication procedure, the environmental conditions (temperature and humidity), and the experimental parameters (indentation rate and preload) on the adhesion results were first tested and later carefully controlled to allow meaningful comparison of data obtained from different specimens. The time elapsed between the fabrication process and the adhesion measurements were critical for reproducibility. Changes in humidity can also influence the experimental P_{ad} values, as liquid bridges around the contact areas result in higher adhesion. Meniscus forces on patterned surfaces depend on the geometry and radius of the contact surfaces, the hydrophobicity of the materials.[48] Adhesion is generally obtained by the amount of force necessary to separate two surfaces in contact and the results (Figure 10a). It is observed that the adhesive forces are closely related to the aspect ratio and duty ratio of nanopillar structure of PS-b-PNIPAAm brushes and, also, are influenced strongly by the thermally responsive property of PNIPAAm as shown in Figure 10b and c. For the adhesive force values, there is a decrease abruptly on the pillars of PS-b-PNIPAAm surface during increasing temperature from 25 to 50 °C. At 25 °C, the adhesive forces of the copolymer pillars increase with the aspect ratio for the duty ratio from 1 to 3. Above duty ratio of 4, it is seen that adhesive force does not vary significantly with the aspect ratio. The adhesive force increases slightly with the aspect ratio for patterned surfaces until a plateau is reached. Among the copolymer surfaces with pillar textures, P(1.5−1) shows the largest adhesive force at 25 °C due to the largest solid fraction of hydrophilic property of the PNIPAAm. At 50 °C, the adhesive forces of the pillars of PS-b-PNIPAAm decrease rapidly with the aspect ratio for the duty ratio from 1 to 3, corresponding to the previous report.[36] Pillar structure with the highest aspect ratio and the lowest duty ratio always shows the lowest adhesive force. Above a duty ratio of 4, it is seen that adhesive force decreases significantly with the aspect ratio for patterned surfaces until a plateau is reached. P(1.5−1) with the highest aspect ratio and the lowest duty ratio shows the lowest adhesive force at 50 °C, consistent with the theoretical prediction of the Cassie model. The thermally responsive efficiency ($\Delta P_{eff} = P_{ad,25°C} - P_{ad,50°C}$) of the adhesive force of copolymer-modified Si surfaces was obtained from calculating adhesive force at 25 and 50 °C. Compared with the flat PS-b-PNIPAAm surface, the PS-b-PNIPAAm pillar array greatly generated the thermally responsive efficiency of the adhesive forces. The adhesive force of the tethered copolymer brushes for P(1.5−1) decreased from 89.4 ± 5 to 8.7 ± 5 nN upon increasing the temperature from 25 to 50 °C; it returned to 83.4 ± 5 nN after decreasing temperature from 50 to 25 °C, this thermally switchable behavior of the copolymer pillar was reversible for 5 cycles. (Figure 9d). P(1.5−1) shows the largest thermally responsive efficiency of the adhesive force. However, the behavior of the copolymer brushes pillar for P(0.25−6) and flat surface of PS-b-PNIPAAm copolymer brushes was unobvious. The results suggest that the thermally switchable efficiency of adhesive force of PS-b-PNIPAAm pillar could be enhanced by increasing the aspect ratio and fractional surface coverage. The advantage of the thermally switchable adhesion described here is the potential to biomimic foot pad of lizards with the ability of alternately attaching and detaching from a surface where they climb. It is well-established that adhesive force is determined by two important factors: contact interfacial forces and noncontact forces such as van der Waals, electrostatic forces, and capillary/meniscus forces.[49] At first, the adhesive force is closely related to the real contact area between the tip and surface; a larger area leads to a larger adhesive force. With the increase in pillar height and fractional surface coverage, the tip traveling between the pillars results in the decrease of the contact area, responsible for decreased adhesive force.[50] Second, when the solid surfaces were hydrophilic, they would easily form a meniscus by the adsorbed water molecules, thus they had larger adhesive forces. However, when the surfaces were hydrophobic, they would show lower adhesion.[51] A PNIPAAm brush at 50 °C increases the surface hydrophobicity of pillar copolymer surfaces, which leads to the reduction of adhesive force. Therefore, surface textures and contact area of thermally responsive property were combined that can be used to generate biomimetic analogues.

To investigate the biological attachment and detachment property, we measured the friction force on the copolymer pillar surface with various aspect ratios and fractional surface coverage of PS-b-PNIPAAm pillar under a normal load of 200 nN by AFM/FFM at 25 and 50 °C, respectively. The friction force is given here in the form of voltage signal, which is proportional to the real friction force.[52] Therefore, the results from various surfaces could be compared to each other. Reproducibility for friction forces is ±3% for all measurements under a normal load of 200 nN. For P(1.5−1) of the copolymer brushes, the results are shown in Figure 11a. As seen from Figure 11a, friction force data also follows a similar trend to the adhesion data for the aspect ratios at 25 and 50 °C. There is an increase when the aspect ratio increases due to the increased contact area of hydrophilic PNIPAAm between the tip and pillars at 25 °C. At 50 °C, the friction force of the PS-b-PNIPAAm pillar decrease rapidly with the aspect ratio due to the hydrophobic property of PNIPAAm (Figure 11a). Compared with the flat PS-b-PNIPAAm surface, the tethered copolymer with pillar textures obviously generated the thermally switchable friction forces. The real area of contact and surface chemistry affect friction force at nanoscale in dry/wet contacts strongly.[52] The real area of contact is dependent upon the area density and height of nanopillars. With the same tip scan velocity, increasing of aspect ratio and fractional surface coverage (duty ratio), the number of asperities in contact is reduced greatly which lead to the real area of contact reduced and so lead to low friction force. Then, if the surface is hydrophilic, it is easy to form capillary meniscus by them or the adsorbed water molecules, which would lead to large shearing strength and higher friction.[51] In other words, if the surface is hydrophobic, it would get the opposite result. The contact regime of PNIPAAm made the surface more hydrophilic and hydrophobic which lead to higher and lower surface energy at 25 and 50 °C, respectively, so P(1.5−1) showed the largest difference of friction force between 25 and 50 °C among the nanotextured surfaces investigated in this study. This thermally switchable behavior of the tethered copolymer pillar for P(1.5−1) on friction force was reversible for 5 cycles (Figure 11b). Without texture structure of the tethered copolymer brushes, the reversibly thermally responsive behavior on friction force was irregular. The mechanism responsible for the obtained inaccuracy may be "stick−slip" phenomenon, in which, during

dx.doi.org/10.1021/jp301068k | J. Phys. Chem. C 2012, 116, 6980−6992

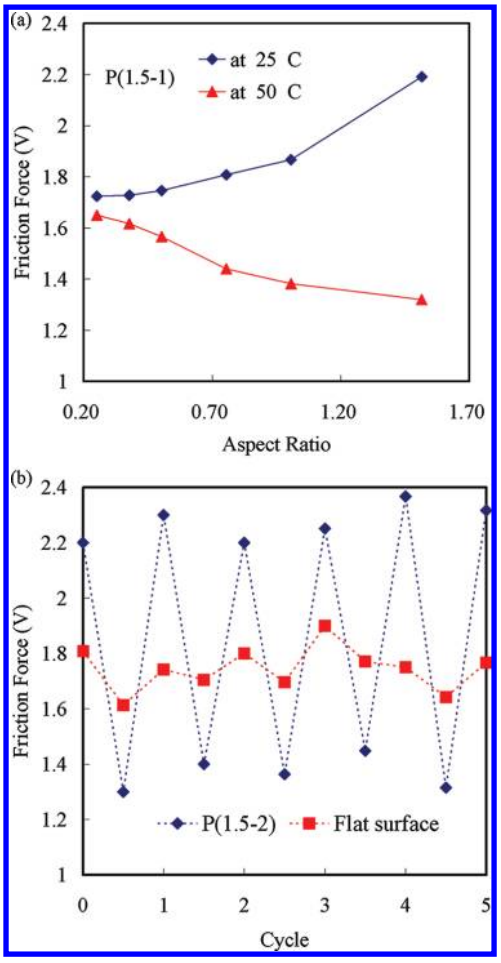

Figure 11. (a) Dependence of the friction force under a normal load of 200 nN on patterned surfaces of P(1.5−1) with pillars of various aspect ratios at 25 and 50 °C. (b) Friction forces on P(1.5−1) and flat surface of the tethered PS-b-PNIPAAm after 5 cycles tuning temperature between 25 and 50 °C.

the stick phase, the friction force builds up to a certain value and, once a large enough force has been applied to overcome the static friction force, slip occurs at the interface.

CONCLUSIONS

In summary, we have used the "grafting from" system with ATRP to prepare a well-defined pillar array of the tethered PS-b-PNIPAAm brushes with various aspect and duty ratios on the Si surface by a lithography process. The copolymer surfaces with nanohierarchical structures were designed to generate attaching and detaching alternately by thermally switchable adhesion or friction force. The effects of nanoscale roughness (aspect ratio of nanopillar and pillar fractional surface coverage) and temperature on the adhesive and nanotriboloogical performance of surfaces were investigated systematically. The results show that thermally switchable performance of the copolymer pillars on adhesion could be apparently enhanced by the copolymer. It is expected that this paper could provide additional insight on the biomimetic foot pad by tailoring the surface topography and using stimuli-responsive hydrogels as the contact regime.

AUTHOR INFORMATION

Corresponding Author

*Tel.: +886-2-27376523. Fax: +886-2-27376544. E-mail: jkchen@mail.ntust.edu.tw.

Notes

The authors declare no competing financial interest.

ACKNOWLEDGMENTS

We thank the National Science Council of the Republic of China and National Nano Device Laboratory for supporting this research financially and the electron beam lithography, respectively.

REFERENCES

(1) Autumn, K.; Liang, Y. A.; Hsieh, S. T.; Zesch, W.; Chan, W. P.; Kenny, T. W.; Fearing, R.; Full, R. J. *Nature* **2000**, *405*, 681−685.
(2) del Campo, A.; Greiner, C.; Arzt, E. *Langmuir* **2007**, *23*, 10235−10243.
(3) del Campo, A.; Greiner, C.; Alvarez, I.; Arzt, E. *Adv. Mater.* **2007**, *19*, 1973.
(4) Northen, M. T.; Turner, K. L. *Nanotechnology* **2005**, *16*, 1159−1166.
(5) Autumn, K.; Hsieh, S. T.; Dudek, D. M.; Chen, J.; Chitaphan, C.; Full, R. J. *J. Exp. Biol.* **2006**, *209*, 260−272.
(6) Huber, G.; Gorb, S. N.; Spolenak, R.; Arzt, E. *Biol. Lett.* **2005**, *1* (1), 2−4.
(7) Greiner, C.; del Campo, A.; Arzt, E. *Langmuir* **2007**, *23*, 3495−3502.
(8) Kim, S.; Aksak, B.; Sitti, M. *Appl. Phys. Lett.* **2007**, *91*, 221913.
(9) Kim, S.; Sitti, M. *Appl. Phys. Lett.* **2006**, *89*, 261911.
(10) Geim, A. K.; Dubonos, S. V.; Grigorieva, I. V.; Novoselov, K. S.; Zhukov, A. A.; Shapoval, S. Y. *Nat. Mater.* **2003**, *2* (7), 461−463.
(11) Yurdumakan, B.; Raravikar, N. R.; Ajayan, P. M.; Dhinojwala, A. *Chem. Commun.* **2005**, *30*, 3799−3801.
(12) Zhao, Y.; Tong, T.; Delzeit, L.; Kashani, A.; Meyyappan, M.; Majumdar, A. *J. Vac. Sci. Technol. B* **2006**, *24* (1), 331−335.
(13) Aksak, B.; Murphy, M. P.; Sitti, M. *Langmuir* **2007**, *23*, 3322−3332.
(14) Shahsavan, H.; Zhao, B. *Langmuir* **2011**, *27*, 7732−7742.
(15) Zeng, H.; Pesika, N.; Tian, Y.; Zhao, B.; Chen, Y.; Tirrell, M.; Turner, K. L.; Israelachvili, J. N. *Langmuir* **2009**, *25* (13), 7486−7495.
(16) Martines, E.; Seunarine, K.; Morgan, H.; Gadegaard, N.; Wilkinson, C. D. W.; Riehle, M. O. *Nano Lett.* **2005**, *5*, 2097−2103.
(17) Patankar, N. A. *Langmuir* **2004**, *20*, 8209−8213.
(18) Northen, M. T.; Turner, K. L. *Nanotechnology* **2005**, *16*, 1159−1166.
(19) Cho, W. K.; Choi, I. S. *Adv. Funct. Mater.* **2008**, *18*, 1089−1096.
(20) Chen, J. K.; Chan, C. H.; Chang, F. C. *Appl. Phys. Lett.* **2008**, *92*, 053108.
(21) Chen, J.-K.; Li, J.-Y. *Appl. Phys. Lett.* **2010**, *97*, 063701.
(22) Chen, J.-K.; Bai, B.-J.; Chang, F.-C. *Appl. Phys. Lett.* **2011**, *99*, 013701.
(23) Chen, J. K.; Zhuang, A. L. *Colloid Polym. Sci.* **2011**, *289*, 1283−1294.
(24) Peppas, N. A.; Hilt, J. Z.; Khademhosseini, A.; Langer, R. *Adv. Mater.* **2006**, *18* (11), 1345−1360.
(25) Chan, C. H.; Chen, J. K.; Chang, F. C. *Sensors Actuators B* **2008**, *13*, 327−332.
(26) Zhao, B.; Brittain, W. J. *Prog. Polym. Sci.* **2000**, *25*, 677−710.
(27) Zhao, B.; Brittain, W. J. *J. Am. Chem. Soc.* **1999**, *121*, 3557−3558.
(28) Rowe, M. A.; Hammer, B. A. G.; Boyes, S. G. *Macromolecules* **2008**, *41*, 4147−4157.
(29) Chen, J.-K.; Chen, Z.-Y.; Lin, H.-C.; Hong, P.-D.; Chang, F.-C. *ACS Appl. Mater. Interfaces* **2009**, *1* (7), 1525−1532.
(30) Chen, J.-K.; Hsieh, C.-Y.; Huang, C.-F.; Li, P.-M. *J. Colloid Interface Sci.* **2009**, *338*, 428−434.

(31) Chen, J. K.; Zhuang, A.-L. *J. Phys. Chem. C* **2010**, *114*, 11801−11809.
(32) Chen, J.-K.; Li, J.-Y. *Sens. Actuators B* **2010**, *150*, 314−320.
(33) Chen, T.-Y.; Chen, J.-K. *Colloid Polym. Sci.* **2011**, *289*, 433−445.
(34) Chen, J. K.; Chen, T.-Y. *J. Colloid Interface Sci.* **2011**, *355*, 359−367.
(35) Li, Gu.; Fan, J.; Jiang, R.; Gao, Y. *Chem. Mater.* **2004**, *16* (10), 1835−1837.
(36) Zhao, W.; Wang, L.; Xue, Q. *ACS Appl. Mater. Interfaces* **2010**, *2*, 788−794.
(37) Tsukruk, V. V.; Bliznyuk, V. N. *Langmuir* **1998**, *14*, 446−455.
(38) Gao, L. C.; McCarthy, T. J. *Langmuir* **2006**, *22*, 6234.
(39) Wenzel, R. N. *Ind. Eng. Chem.* **1936**, *28*, 988.
(40) Cassie, A. B. D.; Baxter, S. *Trans. Faraday Soc.* **1944**, *40*, 546.
(41) Sun, T.; Wang, G.; Feng, L.; Liu, B.; Ma, Y.; Jiang, L.; Zhu, D. *Angew. Chem., Int. Ed.* **2004**, *43*, 357−360.
(42) Chen, J.-K.; Bai, B.-J.; Chang, F.-C. *J. Phys. Chem. C* **2011**, in press.
(43) Chen, J. K.; Hsieh, C. Y.; Huang, C. F.; Li, P. M.; Kuo, S. W.; Chang, F. C. *Macromolecules* **2008**, *41*, 8729−8736.
(44) Rowe, M. A.; Hammer, B. A. G.; Boyes, S. G. *Macromolecules* **2008**, *41*, 4147−4157.
(45) Gil, E. S.; Hudson, S. A. *Prog. Polym. Sci.* **2004**, *29*, 1173−1222.
(46) Yeh, K.-Y.; Chen, L.-J. *Langmuir* **2008**, *24*, 245−251.
(47) Li, L.; Zhu, Y.; Li, B.; Gao, C. *Langmuir* **2008**, *24*, 13632−13639.
(48) Mo, Y. F.; Zhao, W. J.; Huang, D. M.; Zhao, F.; Bai, M. W. *Ultramicroscopy* **2009**, *109*, 247−252.
(49) Burton, Z.; Bhushan, B. *Nano Lett.* **2005**, *5* (8), 1607−1613.
(50) Rabinovich, Y. I.; Adler, J. J.; Ata, A.; Singh, R. K.; Moudgil, B. M. *J. Colloid Interface Sci.* **2000**, *232*, 17−24.
(51) Zhao, W. J.; Zhu, M.; Mo, Y. F.; Bai, M. W. *Colloids. Surf. A* **2009**, *332*, 78−82.
(52) Song, S. Y.; Ren, S. L.; Wang, J. Q.; Yang, S. R.; Zhang, J. Y. *Langmuir* **2006**, *22*, 6010−6015.